Inorganic Chemistry

Article

pubs.acs.org/IC

A Dense I^1O^3 Hybrid Superhydrophobic Network, Pb(H-BTMB), Exhibits Selectivity toward CO_2 Gas Sorption

Koya Prabhakara Rao,*[,†] Yerraguntla Katyayani Devi,[†] Jettiboina Suryachandram,[†] Rayavarapu Prasada Rao,[‡] and J. N. Behera[§]

[†]New Generation Materials Lab (NGML), Department of Science and Humanities, Vignan's Foundation for Science Technology and Research (VFSTR) University, Vadlamudi, Guntur 522213, Andhra Pradesh, India

[‡]Department of Materials Science and Engineering, National University of Singapore (NUS), Singapore 117575, Singapore

[§]School of Chemical Sciences, National Institute of Science Education and Research (NISER), Bhubaneswar 752050, Odisha, India

Supporting Information

ABSTRACT: We achieved a dense I^1O^3 hybrid superhydrophobic porous coordination polymer (PCP), [Pb(H-BTMB)(DMF)] (**1**), by solvothermal methods. The single-crystal XRD structure of **1** indicated that it has a three-dimensional M−L−M framework with one-dimensional M−O−M connectivity leading to an I^1O^3 network. The new PCP obtained exhibited open metal sites (OMSs) by losing a coordinated DMF molecule. The degassed phase displayed selective adsorption of CO_2 gas over N_2, C_2H_6, and C_2H_4 gases. Additionally, it has a superhydrophobic surface with a contact angle of 156.4° at room temperature and it is stable even at 90 °C, displaying a contact angle of 135.3°.

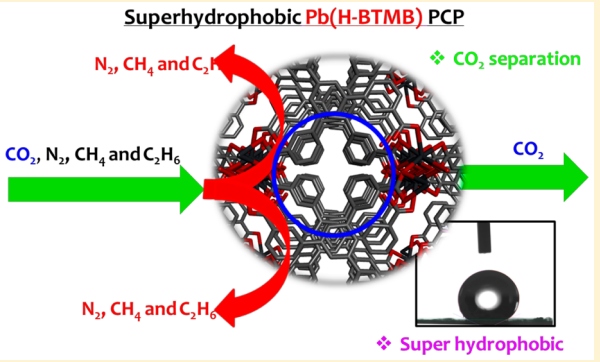

INTRODUCTION

Porous coordination polymers (PCPs), which are also known as metal−organic frameworks (MOFs), are an emerging class of porous solids[1−4] in recent years. These interesting solids can be synthesized by joining the inorganic structural building components (nodes) with organic ligands (linkers). The organic linkers can be tailored with a variety of coordinating functional groups such as carboxylate[1] ($R-COO^-$), phosphonate[2] ($R-PO_3^{2-}$), sulfonate[3] ($R-SO_3^-$) and other organic halo ligands[4] (R−X) through organic synthesis. Recent studies[5,6] have demonstrated that PCPs with the aforementioned permutation of variety in design ability and structural diversity led to extensive development in their applications to gas storage/separation, catalysis, etc.

It is well-known that the structural dimensionality of PCPs/MOFs plays a substantial role in dictating their properties and applications. The structural dimensionality of PCPs/MOFs can be classified[7] on the basis of their inorganic metal−oxygen−metal (M−O−M) bonds and organic metal−ligand−metal (M−L−M) framework. PCPs/MOFs can exhibit I^mO^n (n, m = 0−3) network topology, where "I" refers to the dimensionality of the inorganic M−O connectivity and "O" refers to the M−L connectivity of the organic moiety. The archetypal framework PCP/MOFs, such as the $[Zn_4O(L)_n]$ family,[8] can be classified as having an I^0O^3 framework. In these types of PCP/MOFs, no extended inorganic M−O−M bonds are present, whereas organic ligands link isolated metal centers or metal clusters in all three dimensions of the crystal structures. In fact, the inorganic connectivity affords higher dimensionality (I^1O^n, I^2O^n, and I^3O^n) to the frameworks, which are postulated to have greater thermal, chemical, and magnetic properties.[9] The majority of PCP/MOFs reported in the literature are of I^0O^3 framework type, in which the metal ions coordinated to solvent molecules in pristine form are unstable after removing the guest molecules.[10] Higher dimensionalities in exclusively either inorganic connectivity (I^1O^0, I^2O^0, and I^3O^0) or organic connectivity (I^0O^1, I^0O^2, and I^0O^3) have been commonly reported. However, the synthesis of porous frameworks having higher dimensionality in both inorganic and organic connectivity in a single framework such as I^1O^{1-3}, I^2O^{1-3}, and I^3O^{1-3} is still a significant challenge.[9] Especially I^2O^3, I^3O^2, and I^3O^3 type frameworks are difficult to synthesize and are rather scarce.

In our present study, we focused on higher dimensionality in both inorganic (M−O−M bonds) and organic connectivity (M−L−M links) framework with I^nO^m type porous solids. PCPs having better thermal and chemical stability with open metal sites (OMSs) for selective gas storage/separation and catalysis are the main objectives of our study.[2e,5e,10a] Recently, we have reported[11] the first superhydrophobic PCP, PESD−1, with strong OMSs, containing a Zn(II) metal ion and an asymmetric ligand, benzene-1,3,5-tris(*m*-benzoic acid) (H_3BTMB). Now we focus on other transition elements and

Received: June 19, 2017

DOI: 10.1021/acs.inorgchem.7b01551
Inorg. Chem. XXXX, XXX, XXX−XXX

post-transition elements such as Pb^{2+} due to their inert pair effect.

Herein, we report a new dense I^IO^3 framework, [Pb(H-BTMB)(DMF)] (**1**), with three-dimensional M−L−M connectivity and one-dimensional M−O−M bonds, which displays selectivity toward CO_2 adsorption. We also report the superhydrophobic properties of this new PCP with temperature-dependent contact angle measurements.

EXPERIMENTAL SECTION

Synthesis of [Pb(H-BTMB)(DMF)] (1). A solid mixture of H_3BTMB[12] (11 mg, 0.025 mmol), benzoic acid (12.21 mg, 0.1 mmol), and $Pb(NO_3)_2$ (15.16 mg, 0.038 mmol) was dissolved in a DMF/MeOH/H_2O mixture (0.5/0.25/0.25 mL) in a 2 mL glass vial (Scheme 1). Benzoic acid was used to lower the nucleation of crystal

Scheme 1. Synthesis of [Pb(H-BTMB)(DMF)] Using Solvothermal Conditions

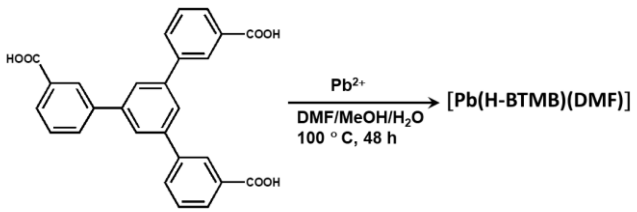

growth in order to achieve a better quality of the single crystals. A 20 μL portion of NaOH (0.01 M) was added as a deprotonating agent, and the initial pH was ∼6.0. The whole reaction mixture was heated in a temperature-controllable oven from room temperature to 100 °C, over a period of 4 h, and then at 100 °C for 48 h. The oven was cooled from 100 °C to room temperature naturally. The product contains homogeneous colorless block-shaped crystals, which were isolated by washing with MeOH and drying in air. Yield: 13.7 mg, 83% based on H_3BTMB (Scheme 1). Anal. Calcd for [Pb(H-BTMB)(DMF)] (≡$C_{30}H_{23}NO_7Pb$): C, 50.27; H, 3.23; N, 1.95. Found: C, 50.18; H, 3.19; N, 1.91. FT-IR (4000−400 cm^{-1}): 3750 (w), 3055 (w), 1647(w), 1586 (w), 1523 (vs), 1457(w), 1408 (m), 1368 (vs), 1275 (m), 1240 (m), 1162 (w), 913 (m), 866 (m), 808 (s), 759 (vs), 680 (vs), 619 (m), 520 (m), 416 (s).

General Characterization Techniques. Thermogravimetric analysis was carried out using a Rigaku TG8120 instrument under flowing nitrogen with a 10 K min^{-1} ramp rate. Powder X-ray diffraction (PXRD) was obtained using a Rigaku RINT powder diffractometer with Cu Kα radiation. Gas adsorption isotherms were obtained using a Belsorp Mini volumetric adsorption instrument (BEL JAPAN Inc.). FTIR spectra were recorded at 298 K with a Cary 639 FTIR instrument with Diamond ATR (Agilent Technologies, USA).

Temperature-Dependent PXRD. The temperature-dependent PXRD measurements were carried out using Cu Kα radiation on a PANalytical X'Pert PRO X-ray diffractometer in the 2θ range of 5−40° with a nominal scan rate of 120 s $step^{-1}$ and a step size of 0.016° from room temperature to 300 °C. The powder sample was pressed into a 6 mm pellet and mounted on an amorphous silicon substrate to avoid background peaks.

Contact Angle Measurements. Contact angles were measured on powder samples using a HOLMARC contact angle meter with rotatable substrate holder, automated dispenser, and temperature control (Model No. HO-IAD-CAM-01B, Holmarc Opto-Mechtronics Ltd., India). The powder samples (∼20 mg) were spread on an aluminum substrate bed and pressed with the help of a glass slide to make a flat surface. On the pressed powder samples, a 20 μL water droplet was released slowly by using an automated 100 μL dispenser. The droplet image was recorded with a high-performance CCD sensor. Drop Snake analysis which is based on B-spline snake to shape the drop was used to analyze the contact angles. Similarly, high-temperature contact angles were measured at room temperature to 90 °C with 10 °C step intervals by heating the substrate bed with a controller. At high temperature, the contact angles were measured quickly (∼5 min) after dropping the water droplet on the surface of the powder sample due to water evaporation phenomena.

RESULTS AND DISCUSSION

Structural Description of 1. Single-crystal XRD analysis of **1** reveals that it crystallizes in the space group *Pccn* (No. 56) (Table S1 in the Supporting Information). The asymmetric unit contains one crystallographically distinct Pb^{2+} ion, one $HBTMB^{2-}$ ligand moiety, and one coordinated DMF solvent molecule (Figures 1 and 2). The crystal structure of **1** has

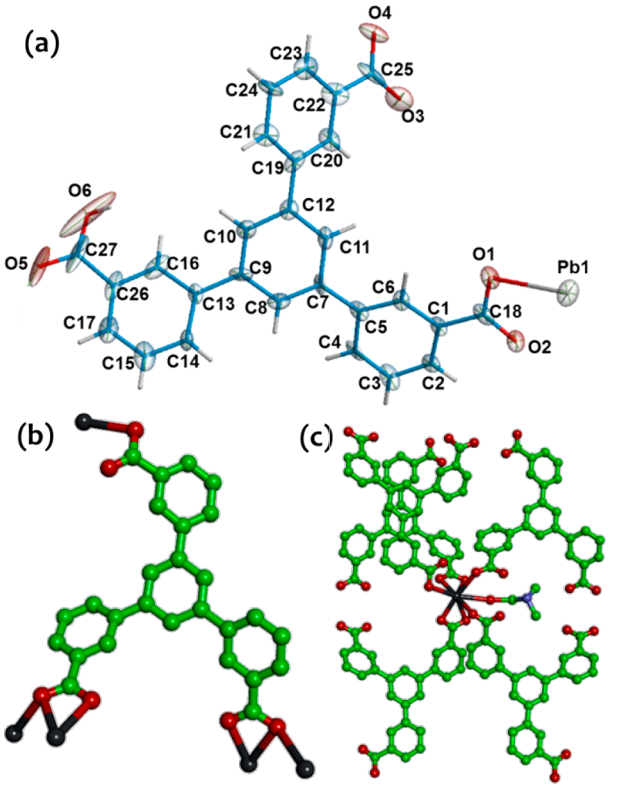

Figure 1. Single-crystal X-ray structures of [Pb(H-BMTB)(DMF)]: (a) ORTEP diagram (50% probability; solvent DMF molecule omitted for clarity); (b) connectivity nodes of three carboxylate (COO^-) moieties with the Pb^{2+} ion; (c) coordination geometry of the Pb^{2+} ion with five different $(H\text{-}BMTB)^{2-}$ ions and a solvent DMF molecule.

three-dimensional (M−L−M framework) organic connectivity with one-dimensional inorganic connectivity (M−O−M) to lead to the I^IO^3 framework. Each Pb^{2+} ion is eight-coordinated to seven oxygen atoms (O(2), O(2)′, O(4), O(4)′, O(1), O(3), O(5)) of five different $HBTMB^{2-}$ ligand moieties. Each Pb^{2+} ion is connected to an adjacent Pb^{2+} ion by edge sharing of O(2)−O(4) of two different $HBTMB^{2-}$ moieties to form a PbO_7 chain along the *c* axis (Figure 2). The Pb−O bond distances vary from 2.456 to 2.942 Å, with the longest bond being from the Pb^{2+} ion to the coordinated DMF solvent. Each Pb^{2+} ion is coordinated to one DMF molecule in pristine form, which can be an open metal site (OMS) available for guest interaction after removing the solvent molecule. Each crystallographically distinct $HBTMB^{2-}$ moiety has three carboxylate moieties connected to Pb^{2+} ions through only five oxygen atoms (O(1)−O(5)); the sixth oxygen atom O(6) is not

DOI: 10.1021/acs.inorgchem.7b01551
Inorg. Chem. XXXX, XXX, XXX−XXX

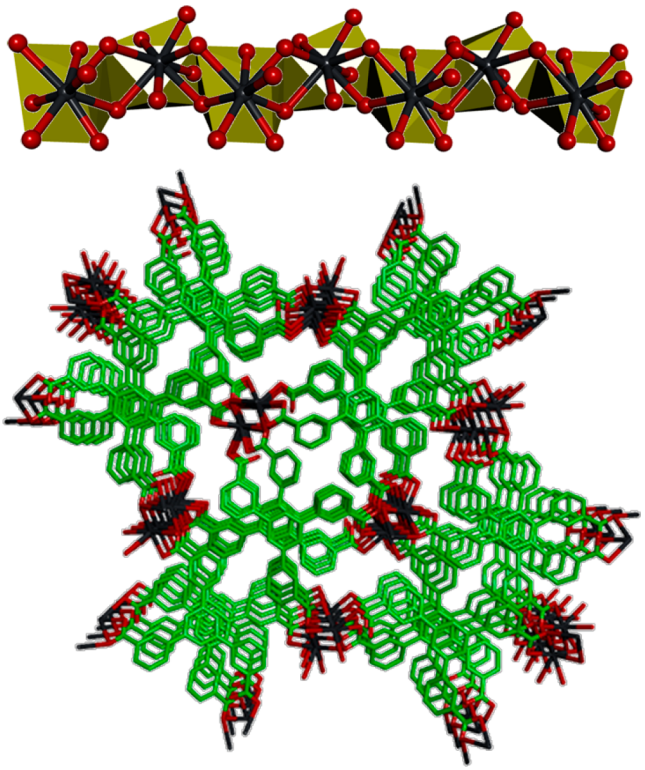

Figure 2. Single-crystal X-ray structures of [Pb(H-BMTB)(DMF)]: (top) PbO_7 one-dimensional chain; (bottom) three-dimensional packing diagram, viewed along the *c* axis. Color scheme: green, carbon; red, oxygen; dark gray, lead.

coordinated to the Pb^{2+} ion. Out of five coordinated oxygen atoms, the two oxygen atoms O(4) and O(2) have μ_3 connectivity[13] and the remaining three oxygen atoms O(1), O(3), and O(5) have μ_2 connectivity[13] (Figure 1).

Powder X-ray Diffraction (PXRD) and Thermogravimetric Analysis (TGA). The PXRD pattern (Figure S1 in the Supporting Information) of **1** is in reasonable agreement with the simulated pattern on the basis of the single-crystal data, indicating that the samples produced were phase pure. Upon degassing of **1** at 275 °C, the PXRD pattern indicated that it is crystalline and similar to that of the parent **1**. As a result, we could conclude that **1** is stable even after removing the coordinated DMF molecule. Thermogravimetric analysis (TGA) of **1** at 723 K shows a four-step isotherm (Figure S2 in the Supporting Information). The first step observed at ~300 °C is due to the loss of a coordinated DMF solvent molecule. The framework is stable up to ~350 °C, and after that it starts to undergo decomposition. On the basis of TGA analysis, the coordinated DMF molecule can be removed at around 300 °C; heating the PCPs/MOFs under these extreme conditions may lead to collapse of the structure. In this context, in the parent sample of **1**, the coordinated DMF was exchanged with methanol by soaking for 3 days with changes of the fresh methanol solvent twice a day. The methanol-exchanged sample of **1** was activated at 275 °C (indicated by TGA, Figure S2); this temperature was used for all characterization measurements, including adsorption studies and contact angle measurements. The stability of the [Pb(H-BMTB)(DMF)] framework was also confirmed by temperature-dependent PXRD data measured on powder samples from room temperature to 300 °C (Figure 3). The PXRD pattern is shown in Figure 3,

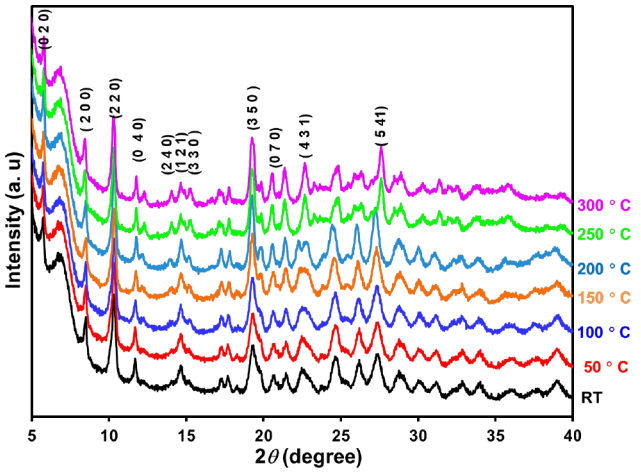

Figure 3. PXRD pattern of [Pb(H-BMTB)(DMF)] in the 2θ range of 5−40° from room temperature to 300 °C (note: a broad peak between 6 and 8° of 2θ is due to an instrument background peak).

showing that the framework could be stable up to 300 °C, in agreement with TGA data. Moreover, all of the major peaks could be indexed on the basis of the single-crystal data of **1** (Figure 3 and Figure S1).

Gas Adsorption Studies. The porosity of **1** was estimated to be 11% using PLATON software. To test the porous nature of this present PCP, attempts were made to measure the gas adsorption properties of the methanol-exchanged sample activated at 275 °C. Adsorption measurements of nitrogen gas performed on Pb(H-BTMB) powder samples at 77 K revealed that it does not take up any nitrogen, probably due to micropore size or blocking effects at such a low temperature (Figure 4). The Brunauer− Emmett−Teller (BET) surface area

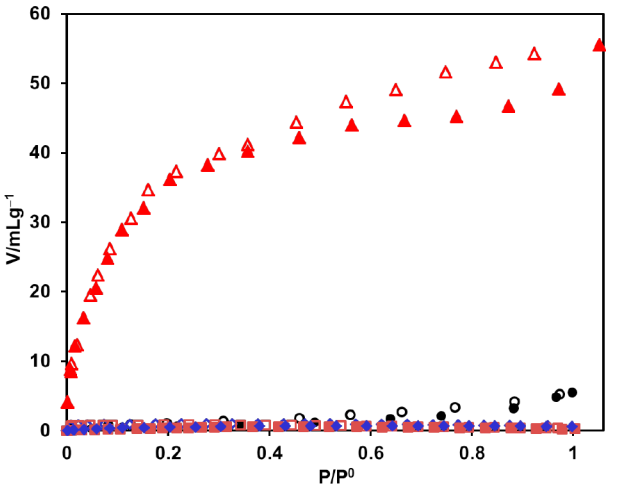

Figure 4. Adsorption isotherms of Pb(H-BTMB) for CO_2 (red), C_2H_4 (brown), and C_2H_6 (blue) at 195 K and for N_2 (black) at 77 K. Filled and open symbols are adsorption and desorption data, respectively.

evaluated from the CO_2 adsorption data 195 K is 155 m^2 g^{-1}, thus indicating that Pb(H-BTMB) has microporosity available for guest inclusion. The adsorption measurements for C_2H_6 and C_2H_4 at 195 K on Pb(H-BTMB) powder samples showed that the compound cannot take up these two gases (Figure 4). Similar adsorption measurements for CO_2, C_2H_6, and C_2H_4 at 273 and 298 K on Pb(H-BTMB) powder samples (Figures S3−

DOI: 10.1021/acs.inorgchem.7b01551
Inorg. Chem. XXXX, XXX, XXX−XXX

S5 in the Supporting Information) also specified that **1** cannot take up C_2H_6 and C_2H_4 gases owing to the large kinetic diameter (CO_2, 3.3 Å; C_2H_6 and C_2H_4, 3.9 Å). The CO_2 adsorption on **1** at the three temperatures 195, 273, and 298 K are 55, 21, and 14 mL (STP) g^{-1}, respectively (Figure S5). From the above adsorption measurements, we conclude that Pb(H-BTMB) can selectively take up CO_2 from C_2H_6 and C_2H_4 gases.

Superhydrophobicity and Temperature Dependence Study. To examine the hydrophobic or hydrophilic properties of **1**, contact angle measurements were performed on as-synthesized and degassed powder samples, separately. The contact angles 156.4 and 155.3° were observed on as-synthesized and degassed powder samples of **1**, respectively, with a roll-off angle of less than 10° (Figure 5 and Figures S6 and S7 in the Supporting Information), which is characteristic of a superhydrophobic solid (self-cleaning or Lotus behavior).[14] Our previously reported[11] superhydrophobic PCP PESD−1, achieved with the same H_3BTMB ligand, displayed similar contact angles. In fact, the crystal structure of PESD−1 is a layered with low-density hydrocarbon moieties exposed to the surface.[11] In contrast to PESD−1, [Pb(H-BTMB)(DMF)], having a dense I^1O^3 hybrid framework with three-dimensional structure, has also been shown to have a superhydrophobic surface even in the degassed state (Figure 5c). This result clearly indicated that the H_3BTMB ligand with an unsymmetrical coordinating functional group (−COOH) at the meta position could be the main reason for the presence of a superhydrophobic surface, though PESD−1[11] and **1** have different crystal structures. On the other hand, similar chemical formulas of H_3BTB ligands forming archetypal framework PCP/MOFs, such as the $[Zn_4O(L)_n]$ family[8] and others,[10a] are hygroscopic. In this context, we carried out similar contact angle measurements on the powder samples of the H_3BTMB ligand itself, to understand more precisely the hydrophobic or hydrophilic properties. Surprisingly, a water droplet does not stay on the surface but is absorbed by the H_3BTMB ligand powder sample (Figure 5a). These results clearly indicated that the organic H_3BTMB ligand is hydrophilic and when it is coordinated to metal ions (Pb^{2+}) it converts to a superhydrophobic surface (Figure 5). Indeed, the H_3BTMB ligand with an unsymmetrical coordinating functional group (−COOH at the meta position) approaches superhydrophobic surfaces. This phenomenon can also be understood by observing the packing arrangements of H_3BTMB ligand molecules in solid crystalline form. H_3BTMB molecules are arranged in a fashion such that the hydrocarbon surface is not oriented in any crystallographic direction (see Figure S9 in the Supporting Information for the X-ray crystal structure of H_3BTMB ligand showing the possible short contacts and hydrogen bonds). Furthermore, this molecular arrangement might lead to strong hydrogen bonds between water molecules and the carboxylic (−COOH) moiety of the H_3BTMB ligand, which might be the reason for the hydrophilic nature of the solid. As expected, the preferential orientation of PXRD in **1** along the (*HK*0) direction due to inorganic PbO_7 chains and more hydrocarbon surfaces dominating along the *c* axis (Figure S10) is open for a guest interactive site (water), which could lead to the hydrophobic surface in **1**. Superhydrophobic PCPs reported earlier,[14] including our report,[11] are precisely low-density hydrocarbon-rich compounds. The title PCP has a dense I^1O^3 hybrid framework, which exhibits a superhydrophobic surface even in the degassed state.

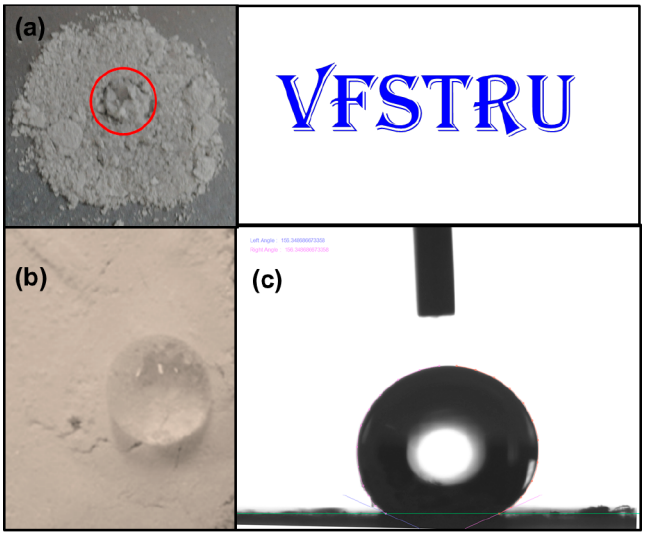

Figure 5. Picture showing a drop of water placed on (a) a powder sample of the H_3BTMB ligand and (b) a powder sample of [Pb(H-BTMB)(DMF)]. (c) Contact angle measured at room temperature on a powder sample of [Pb(H-BTMB)(DMF)].

To understand this peculiar hydrophobic behavior and its temperature-dependent hydrophobicity, we carried out similar contact angle measurements on the powder sample of **1**, at room temperature to 90 °C, at 10 °C temperature intervals (Figures S6 and S7 in the Supporting Information). After the water droplet is dropped on the powder samples, the water will exist as in the form of a droplet as long as water does not evaporate from the surface, which shows that the hydrophobic nature survives for longer periods. However, the contact angles slightly decreased from 156.4° (at room temperature) to 135.3° (at 90 °C) (Figure 5 and Figures S6−S8 in the Supporting Information). Nevertheless, the surface converted from superhydrophobic (i.e., >150°) at room temperature to hydrophobic, with a contact angle still as high as 135.3° (at 90 °C). A plot of contact angles vs temperature (Figure S8) indicated that the contact angle decreased almost linearly with negative slope. The slight decrease in contact angle could be due to the fact that at high temperature water vapor started condensing, which reduces the roughness of the surface similar to that of a lotus leaf.[15] Moreover, at high temperature water penetrates through the surface better than at low temperature, leading to low contact angles. In fact, most of the superhydrophobic PCPs could not retain the hydrophobic surface at high temperature, including lotus leaf.[15] To the best of our knowledge, this is the first example accomplishing superhydrophobicity in a dense I^1O^3 hybrid framework without any surface modifications[14e] even at high temperature.

CONCLUSION

In conclusion, we achieved a new dense I^1O^3 hybrid superhydrophobic PCP, **1**, by solvothermal methods. The new PCP obtained has a three-dimensional structure with one-dimensional M−O−M bonds by creating an I^1O^3 network. Moreover, in the pristine form of **1**, the coordinated DMF solvent molecule was lost upon degassing, exhibiting OMS with a stable framework. The degassed phase displayed selective adsorption of CO_2 gas over N_2, C_2H_6, and C_2H_4 gases. PCPs with an I^1O^3 network exhibiting OMS with a thermally stable

DOI: 10.1021/acs.inorgchem.7b01551
Inorg. Chem. XXXX, XXX, XXX−XXX

framework are rather scarce. In addition, **1** has a superhydrophobic surface, which is stable even under high-temperature conditions. To the best of our knowledge, this is the first PCP achieving superhydrophobicity with a dense I^1O^3 hybrid network together in a single PCP framework without any surface modifications. This study provides a road map for the design and synthesis of dense porous materials having better thermal and chemical stability with OMSs for better gas interactions, which have a promising role in gas separation and catalysis.

■ ASSOCIATED CONTENT

Supporting Information

The Supporting Information is available free of charge on the ACS Publications website at DOI: 10.1021/acs.inorgchem.7b01551.

Syntheses, details of the experiments and instruments, X-ray structural parameters, X-ray powder patterns, thermogravimetric analysis, gas adsorption study, contact angle measurements, and X-ray crystal structures (PDF)

Accession Codes

CCDC 1563237−1563238 contain the supplementary crystallographic data for this paper. These data can be obtained free of charge via www.ccdc.cam.ac.uk/data_request/cif, or by emailing data_request@ccdc.cam.ac.uk, or by contacting The Cambridge Crystallographic Data Centre, 12 Union Road, Cambridge CB2 1EZ, UK; fax: +44 1223 336033.

■ AUTHOR INFORMATION

Corresponding Author

*E-mail for K.P.R.: kprao2005@gmail.com, drkpr_sh@vignanuniversity.org.

ORCID

Koya Prabhakara Rao: 0000-0001-6077-5746

Author Contributions

K.P.R. designed and conceded out all the experiments. Y.K.D. and J.S. carried out contact angle measurements and analysis of the samples, and R.P.R. carried out temperature-dependent PXRD experiments. All of the authors contributed in writing the manuscript.

Notes

The authors declare no competing financial interest.

■ ACKNOWLEDGMENTS

This work was financially supported by the DST-SERB, project for early career, project no. EMR/2014/001114. J.S. thanks the DST-SERB for providing a junior research fellowship (JRF).

■ REFERENCES

(1) (a) Yaghi, O. M.; O'Keeffe, M.; Ockwig, N. W.; Chae, H. K.; Eddaoudi, M.; Kim, J. Reticular synthesis and the design of new materials. *Nature* **2003**, *423*, 705−714. (b) Kitagawa, S.; Kitaura, S. R.; Noro, S.-I. Functional porous coordination polymers. *Angew. Chem., Int. Ed.* **2004**, *43*, 2334−2375. (c) Long, J. R.; Yaghi, O. M. The pervasive chemistry of metal−organic frameworks. *Chem. Soc. Rev.* **2009**, *38*, 1213−1214. (d) Férey, G. Hybrid porous solids: past, present, future. *Chem. Soc. Rev.* **2008**, *37*, 191−214. (e) Tan, J. C.; Cheetham, A. K. Mechanical properties of hybrid inorganic−organic framework materials: establishing fundamental structure−property relationships. *Chem. Soc. Rev.* **2011**, *40*, 1059−1080. (f) Lee, J.; Farha, O. K.; Roberts, J.; Scheidt, K. A.; Nguyen, S. T.; Hupp, J. T. Metal−organic framework materials as catalysts. *Chem. Soc. Rev.* **2009**, *38*, 1450−1459. (g) Lian, X.; Fang, Y.; Joseph, E.; Wang, Q.; Li, J.; Banerjee, S.; Lollar, C.; Wang, X.; Zhou, H.-C. Enzyme-MOF (metal-organic framework) composites. *Chem. Soc. Rev.* **2017**, *46*, 3386−3401. (h) Bosch, M.; Yuan, S.; Rutledge, W.; Zhou, H.-C. Stepwise synthesis of Metal-Organic Frameworks. *Acc. Chem. Res.* **2017**, *50*, 857−865.

(2) (a) Finn, R. C.; Zubieta, J.; Haushalter, R. C. Crystal chemistry of organically templated vanadium phosphates and organophosphonates. *Prog. Inorg. Chem.* **2002**, *51*, 421−601. (b) Clearfield, A. Metal-phosphonate chemistry. *Prog. Inorg. Chem.* **1997**, *47*, 371−510. (c) Bao, S. S.; Zheng, L. M.; Liu, Y. J.; Xu, W.; Feng, S. Sodium cobalt aminomethylidenediphosphonate with a novel open framework structure. *Inorg. Chem.* **2003**, *42*, 5037−5039. (d) Rao, K. P.; Vidyasagar, K. Synthesis and X-ray crystal structures of the new, three-dimensional ethylenediphosphonates $[A\{HO_3P(CH_2)_2PO_3H_2\}]$ (A = Alkali Metal, Tl, or NH_4): solid brönsted acids that exhibit topotactic intercalation and deintercalation of ammonia. *Eur. J. Inorg. Chem.* **2006**, *2006*, 813−819. (e) Rao, K. P.; Vidyavathy, B.; Minimol, M. P.; Vidyasagar, K. Hydrothermal synthesis and characterization of new pillared layered ethylenediphosphonates of molybdenum (VI), $A_2[Mo_2O_5(O_3PCH_2CH_2PO_3)]$ (A = NH_4, Tl, Cs, Rb) and $K(H_3O)$-$[Mo_2O_5(O_3PCH_2CH_2PO_3)]$. *Inorg. Chem.* **2004**, *43*, 4610−4614.

(3) (a) Shimizu, G. K. H.; Ramanathan, V.; Taylor, J. M. Phosphonate and sulfonate metal organic frameworks. *Chem. Soc. Rev.* **2009**, *38*, 1430−1449. (b) Chandler, B. D.; Enright, G. D.; Pawsey, S.; Ripmeester, J. A.; Cramb, D. T.; Shimizu, G. K. H. Mechanical gas capture and release in a network solid via multiple single-crystalline transformations. *Nat. Mater.* **2008**, *7*, 229−235. (c) Ribas, X.; Maspoch, D.; Wurst, K.; Veciana, J.; Rovira, C. Coordination capabilities of a novel organic polychlorotriphenylmethyl monosulfonate radical. *Inorg. Chem.* **2006**, *45*, 5383−5392.

(4) Phan, A.; Doonan, C. J.; Uribe-Romo, F. J.; Knobler, C. B.; O'Keeffe, M.; Yaghi, O. M. Synthesis, structure, and carbon dioxide capture properties of zeolitic imidazolate frameworks. *Acc. Chem. Res.* **2010**, *43*, 58−67.

(5) (a) Chui, S. S. -Y.; Lo, S. M. -F.; Charmant, J. P. H.; Orpen, A. G.; Williams, I. D. A chemically functionalizable nanoporous material $[Cu_3(TMA)_2(H_2O)_3]_n$. *Science* **1999**, *283*, 1148−1150. (b) Das, S.; Kim, H.; Kim, K. Metathesis in single crystal: complete and reversible exchange of metal ions constituting the frameworks of Metal−Organic frameworks. *J. Am. Chem. Soc.* **2009**, *131*, 3814−3815. (c) Dincă, M.; Long, J. R. Hydrogen storage in microporous metal-organic frameworks with exposed metal sites. *Angew. Chem., Int. Ed.* **2008**, *47*, 6766−6779. (d) Xiang, S.; Zhou, W.; Gallegos, J. M.; Liu, Y.; Chen, B. Exceptionally high acetylene uptake in a microporous Metal−Organic framework with open metal sites. *J. Am. Chem. Soc.* **2009**, *131*, 12415−12419. (e) Duan, J.; Higuchi, M.; Horike, S.; Foo, M. L.; Rao, K. P.; Kitagawa, S. A family of rare earth porous coordination polymers with different flexibility for CO_2/C_2H_4 and CO_2/C_2H_6 Separation. *Inorg. Chem.* **2013**, *52*, 8244−8249. (f) Meng, Q.; Xin, X.; Zhang, L.; Dia, F.; Wang, R.; Sun, D. A multifunctional Eu MOF as a fluorescent pH sensor and exhibiting highly solvent-dependent adsorption and degradation of rhodamine B. *J. Mater. Chem. A* **2015**, *3*, 24016−24021.

(6) (a) Bloch, E. D.; Queen, W. L.; Krishna, R.; Zadrozny, J. M.; Brown, C. M.; Long, J. R. Hydrocarbon separations in a metal-organic framework with open iron(II) coordination sites. *Science* **2012**, *335*, 1606−1610. (b) Yoon, M.; Srirambalaji, R.; Kim, K. Homochiral Metal−Organic frameworks for asymmetric heterogeneous catalysis. *Chem. Rev.* **2012**, *112*, 1196−1231. (c) Hu, Z.; Nalaparaju, A.; Peng, Y.; Jiang, J.; Zhao, D. Modulated hydrothermal synthesis of UiO-66(Hf)-type metal organic frameworks for optimal carbon dioxide separation. *Inorg. Chem.* **2016**, *55*, 1134−1141. (d) Hu, Z.; Peng, Y.; Kang, Z.; Qian, Y.; Zhao, D. A modulated hydrothermal (MHT) approach for the facile synthesis of UiO-66-Type MOFs. *Inorg. Chem.* **2015**, *54*, 4862−4868. (e) Hu, Z.; Khurana, M.; Seah, Y. H.; Zhang, M.; Guo, Z.; Zhao, D. Ionized Zr-MOFs for highly efficient post-combustion CO_2 capture. *Chem. Eng. Sci.* **2015**, *124*, 61−69. (f) Wang, R.; Zhang, M.; Liu, X.; Zhang, L.; Kang, Z.; Wang, W.; Wang, X.; Dai, F.; Sun, D. Tuning the dimensionality of interpenetration in a pair of framework-catenation isomers to achieve selective adsorption of CO_2

DOI: 10.1021/acs.inorgchem.7b01551
Inorg. Chem. XXXX, XXX, XXX−XXX

and fluorescent sensing of metal ions. *Inorg. Chem.* **2015**, *54*, 6084−6086.
(7) Cheetham, A. K.; Rao, C. N. R.; Feller, R. K. Structural diversity and chemical trends in hybrid inorganic−organic framework materials. *Chem. Commun.* **2006**, 4780−4795.
(8) (a) Chae, H. K.; Siberio-Pérez, D. Y.; Kim, J.; Go, Y. B.; Eddaoudi, M.; Matzger, A. J.; O'Keeffe, M.; Yaghi, O. M. A route to high surface area, porosity and inclusion of large molecules in crystals. *Nature* **2004**, *427*, 523−527. (b) Furukawa, H.; Ko, N.; Go, Y. B.; Aratani, N.; Choi, S. B.; Choi, E.; Yazaydin, A. Ö.; Snurr, R. Q.; O'Keeffe, M.; Kim, J.; Yaghi, O. M. Ultrahigh porosity in metal-organic frameworks. *Science* **2010**, *329*, 424−428.
(9) (a) Foo, M. L.; Horike, S.; Inubushi, Y.; Kitagawa, S. An alkaline earth I^3O^0 porous coordination polymer: $[Ba_2TMA(NO_3)(DMF)]$. *Angew. Chem., Int. Ed.* **2012**, *51*, 6107−6111. (b) Anokhina, E. V.; Vougo-Zanda, M.; Wang, X.; Jacobson, A. J. $In(OH)BDC_{0.75}BDCH_2$ (BDC = Benzenedicarboxylate), a hybrid Inorganic−Organic vernier structure. *J. Am. Chem. Soc.* **2005**, *127*, 15000−15001. (c) Scherb, C.; Schodel, A.; Bein, T. Directing the structure of metal-organic frameworks by oriented surface growth on an organic monolayer. *Angew. Chem., Int. Ed.* **2008**, *47*, 5777−5779. (d) Hu, Z.; Zhang, K.; Zhang, M.; Guo, Z.; Jianwen, J.; Zhao, D. A combinatorial approach towards water-stable metal−organic frameworks for highly efficient carbon dioxide separation. *ChemSusChem* **2014**, *7*, 2791−2795.
(10) (a) Rao, K. P.; Higuchi, M.; Duan, J.; Kitagawa, S. pH-dependent interpenetrated, polymorphic, Cd^{2+}- and BTB-based Porous coordination polymers with open metal sites. *Cryst. Growth Des.* **2013**, *13*, 981−985. (b) Zheng, S. − T.; Wu, T.; Zuo, F.; Chou, C.; Feng, P.; Bu, X. Mimicking zeolite to its core: porous sodalite cages as hangers for pendant trimeric $M_3(OH)$ clusters (M = Mg, Mn, Co, Ni, Cd). *J. Am. Chem. Soc.* **2012**, *134*, 1934−1937.
(11) Rao, K. P.; Higuchi, M.; Sumida, K.; Furukawa, S.; Duan, J.; Kitagawa, S. Design of superhydrophobic porous coordination polymers through the introduction of external surface corrugation by the use of an aromatic hydrocarbon building unit. *Angew. Chem., Int. Ed.* **2014**, *53*, 8225−8230.
(12) He, Y.; Bian, Z.; Kang, C.; Cheng, Y.; Gao, L. Novel C_3-symmetrical triphenylbenzene-based organogelators with different linkers between phenyl ring and alkyl chain. *Tetrahedron* **2010**, *66*, 3553−3563.
(13) Rao, K. P.; Thirumurugan, A.; Rao, C. N. R. Lamellar and three-dimensional hybrid compounds formed by cyclohexene- and cyclohexanedicarboxylates of Pb, La, and Cd. *Chem. - Eur. J.* **2007**, *13*, 3193−3201.
(14) (a) Colombo, V.; Galli, S.; Choi, H. J.; Han, G. D.; Maspero, A.; Palmisano, G.; Masciocchi, N.; Long, J. R. High thermal and chemical stability in pyrazolate-bridged metal−organic frameworks with exposed metal sites. *Chem. Sci.* **2011**, *2*, 1311−1319. (b) Chen, T.-H.; Popov, I.; Zenasni, O.; Daugulis, O.; Miljanic, O. S. Superhydrophobic perfluorinated metal−organic frameworks. *Chem. Commun.* **2013**, *49*, 6846−6848. (c) Wang, Z. Q.; Cohen, S. M. Postsynthetic modification of metal−organic frameworks. *Chem. Soc. Rev.* **2009**, *38*, 1315−1329. (d) Nguyen, J. G.; Cohen, S. M. Moisture-resistant and superhydrophobic Metal−Organic frameworks obtained via postsynthetic modification. *J. Am. Chem. Soc.* **2010**, *132*, 4560−4561. (e) Yang, C.; Kaipa, U.; Mather, Q. Z.; Wang, X. P.; Nesterov, V.; Venero, A. F.; Omary, M. A. Fluorous Metal−Organic frameworks with superior adsorption and hydrophobic properties toward oil spill cleanup and hydrocarbon storage. *J. Am. Chem. Soc.* **2011**, *133*, 18094−18097. (f) Serre, C. Superhydrophobicity in highly fluorinated porous Metal−Organic frameworks. *Angew. Chem., Int. Ed.* **2012**, *51*, 6048−6050. (g) He, C. − T.; Jiang, L.; Ye, Z. − M.; Krishna, R.; Zhong, Z. − S.; Liao, P. − Q.; Xu, J.; Ouyang, G.; Zhang, J. − P.; Chen, X. − M. Exceptional hydrophobicity of a large-pore Metal−Organic zeolite. *J. Am. Chem. Soc.* **2015**, *137*, 7217−7223. (h) Jayaramulu, K.; Datta, K. K. R.; Rösler, C.; Petr, M.; Otyepka, M.; Zboril, R.; Fischer, R. A. Biomimetic superhydrophobic/superoleophilic highly fluorinated graphene oxide and ZIF-8 composites for oil−water separation. *Angew. Chem., Int. Ed.* **2016**, *55*, 1178−1182. (i) Zhang, M.; Xin, X.; Xiao, Z.; Wang, R.; Zhang, L.; Sun, D. A multi-aromatic hydrocarbon unit induced hydrophobic metal−organic framework for efficient C_2/C_1 hydrocarbon and oil/water separation. *J. Mater. Chem. A* **2017**, *5*, 1168−1175.
(15) Cheng, Y. − T.; Rodak, D. E. Is the lotus leaf superhydrophobic? *Appl. Phys. Lett.* **2005**, *86*, 144101−144103.

DOI: 10.1021/acs.inorgchem.7b01551
Inorg. Chem. XXXX, XXX, XXX−XXX